

RESEARCH LETTER

10.1002/2015GL063843

Key Points:

- New framework linking temperature variance to climate feedbacks
- Thermocline feedback and dynamical damping shape patterns of ENSO amplitude
- Diagnostic tool for model biases and ENSO sensitivity assessment

Supporting Information:

- Figures S1–S12

Correspondence to:

J. Boucharel,
j.boucharel@unsw.edu.au

Citation:

Boucharel, J., A. Timmermann, A. Santoso, M. H. England, F.-F. Jin, and M. A. Balmaseda (2015), A surface layer variance heat budget for ENSO, *Geophys. Res. Lett.*, 42, 3529–3537, doi:10.1002/2015GL063843.

Received 16 MAR 2015

Accepted 13 APR 2015

Accepted article online 16 APR 2015

Published online 13 MAY 2015

A surface layer variance heat budget for ENSO

Julien Boucharel¹, Axel Timmermann², Agus Santoso¹, Matthew H. England¹, Fei-Fei Jin^{3,4}, and Magdalena A. Balmaseda⁵
¹ARC Centre of Excellence for Climate System Science, University of New South Wales, Sydney, New South Wales, Australia,

²International Pacific Research Center and Department of Oceanography, University of Hawai'i at Mānoa, Honolulu, Hawaii, USA,

³Department of Atmospheric Sciences, SOEST, University of Hawai'i at Mānoa, Honolulu, Hawaii, USA,

⁴Laboratory for Climate Studies, Beijing Climate Center, Chinese Meteorological Agency, Beijing, China,

⁵European Centre for Medium-Range Weather Forecasts, Reading, UK

Abstract Characteristics of the El Niño–Southern Oscillation (ENSO), such as frequency, propagation, spatial extent, and amplitude, strongly depend on the climatological background state of the tropical Pacific. Multidecadal changes in the ocean mean state are hence likely to modulate ENSO properties. To better link background state variations with low-frequency amplitude changes of ENSO, we develop a diagnostic framework that determines locally the contributions of different physical feedback terms on the ocean surface temperature variance. Our analysis shows that multidecadal changes of ENSO variance originate from the delicate balance between the background-state-dependent positive thermocline feedback and the atmospheric damping of sea surface temperatures anomalies. The role of higher-order processes and atmospheric and oceanic nonlinearities is also discussed. The diagnostic tool developed here can be easily applied to other tropical ocean areas and climate phenomena.

1. Introduction

The El Niño–Southern Oscillation (ENSO) is the largest source of interannual climate variability in the world [McPhaden *et al.*, 1998]. As a result of the large-scale atmospheric response to equatorial sea surface temperature anomalies (SSTA), ENSO has far-reaching tropical and extratropical impacts in both hemispheres [Ashok *et al.*, 2007; Su *et al.*, 2001; Zhang *et al.*, 2012]. ENSO can be regarded as a coupled atmosphere-ocean instability of the climatic background state arising from a tight interplay of positive and negative feedbacks, either amplifying or damping the associated anomalies. This climatological state evolves slowly on decadal and secular timescales, thus impacting the statistical and dynamical properties of ENSO, such as its amplitude and propagation [Fedorov and Philander, 2000; Timmermann, 2001; An *et al.*, 2006; Boucharel *et al.*, 2013; Santoso *et al.*, 2013].

A specific example of secular background changes and potential impacts on ENSO properties is the tropical climate response to greenhouse warming. The current generation of Coupled General Circulation Models (CGCM) predicts on average a future weakening of the Walker circulation and resulting oceanic changes, which include a shoaled, less tilted, and sharper equatorial thermocline, weaker zonal currents and equatorial upwelling, and increased thermal stratification [DiNezio *et al.*, 2009; Vecchi and Soden, 2007; Yeh *et al.*, 2009; Dewitte *et al.*, 2013]. How ENSO will respond to these slowly evolving conditions still remains elusive and model dependent [Bellenger *et al.*, 2013]. In particular, the model-based projections for ENSO amplitude (quantified for instance by the variance of eastern equatorial SSTA) are highly uncertain [Collins *et al.*, 2010; Guilyardi *et al.*, 2012]. Such an uncertainty can arise if compensating feedbacks nearly balance each other [Kim and Jin, 2011]. To quantify the effect of potentially counter-acting feedbacks on changes in ENSO characteristics, various methods have been developed and applied to different background states. These methods include projections onto simplified linearized dynamical models [An *et al.*, 2004; Dewitte *et al.*, 2007] and heat budget-based diagnostics [Jin *et al.*, 2006; DiNezio *et al.*, 2012] for specified key regions. These frameworks are based on linear regressions between temperature, wind, heat fluxes, and ocean current anomalies. Oftentimes, events are composited to evaluate the spatial characteristics of dynamical processes. This composite approach does not readily provide information on the time-evolving nature of ENSO and its change in amplitude on decadal timescales.

Here we develop a new local diagnostic framework that links changes in the climate background state with variance of local near surface ocean temperature anomalies. The method, described in section 2, is

based on the mixed layer (ML) temperature variance equation, which exploits covariance between local temperature anomalies, oceanic and atmospheric changes. Applied to an ocean reanalysis product covering the period 1959–2009, we determine in section 3 the mechanisms that shape mean ENSO variance and its low-frequency variations. Section 4 provides a discussion of our main results, followed by concluding remarks.

2. Data and Method

2.1. Temperature Variance Equation

To investigate the processes that control the local temperature T and its tendency $\partial T/\partial t$, we start with a heat budget equation for the ML temperature similar to Wang and McPhaden [1999]. The total mixed layer heat balance $Q_t = \partial T/\partial t$ can be written as a sum of advective terms, eddy/mixing components, air-sea heat flux contributions Q_{flux} , and an unresolved residual Q_{res} (e.g., which includes for instance shortwave fluxes at the base of the ML):

$$\frac{\partial T}{\partial t} = [-U\partial_x T - V\partial_y T - W\partial_z T + k_l(\partial_{xx} T + \partial_{yy} T) + \partial_z[k_v(z)\partial_z T]] + \frac{Q_{\text{flux}} + Q_{\text{res}}}{\rho_0 c_p h} \quad (1)$$

All surface flux terms are taken as positive when they represent heat gain into the ocean. We use the abbreviations $\partial/\partial x = \partial_x$ and $\partial^2/\partial x^2 = \partial_{xx}$ (same for y, z). U , V , and W represent the depth-averaged mixed layer velocity fields. The density of seawater, ρ_0 , is assumed to be constant at 1022.6 kg/m^3 ; so too is the ocean heat capacity, c_p , taken as $3940 \text{ J kg}^{-1} \text{ K}^{-1}$. The net surface heat flux across the air-sea interface (Q_{flux}) is composed of the shortwave solar radiation (Q_{short}), outgoing longwave radiation (Q_{long}), latent heat flux (Q_{latent}), and sensible heat flux (Q_{sensible}). Most of heat budget analysis with a specific focus on the equatorial Pacific variability and in particular ENSO assume a 50m constant ML depth as motivated by the Cane and Zebiak model for ENSO [Zebiak and Cane, 1987], and the results are not sensitive to variations up to $\pm 20 \text{ m}$ in the choice of depth [e.g., Cai et al., 2015]. The ML depth in the eastern equatorial Pacific is around 20 m. Integrating over a layer deeper than 30 m would mix thermocline and mixed layer dynamics in the Eastern Pacific and obscure the physical interpretation in this key ENSO region. So, we opt for a constant surface layer depth $h = 25 \text{ m}$, as a time evolving mixed layer would require a Taylor expansion of h and would add considerable complexity to our framework (see supporting information for results from a deeper layer integration). The mixing terms, due to lateral turbulent heat diffusion are parameterized using a lateral diffusivity coefficient $k_l = 0.05 \times 10^4 \text{ m}^2/\text{s}$. To capture vertical mixing, we use an eddy diffusion model (the so-called K-Profile Parameterization, KPP), derived for the equator at 110°W [Li et al., 2001, Figure 1c]. To gain more insight into advective processes, we break up temperatures, velocities, and heat fluxes into monthly stratified long-term means and interannual anomalies as follows: $X = \bar{X} + X'$ with $X = T, U, V, W$, or Q , where overbar denotes monthly stratified mean and prime denotes the interannual anomalies (relative to the long-term mean climatology). Discretizing the vertical temperature gradient as $\partial T/\partial z = (T - T_{\text{sub}})/\Delta h$ with $\Delta h = z_{\text{sub}} - h/2$ and T_{sub} the temperature below the surface layer (at the z_{sub} depth), we obtain

$$\frac{\partial T'}{\partial t} = \left[\begin{aligned} & -\bar{U}\partial_x T' - \bar{V}\partial_y T' - \bar{W}\frac{T'}{\Delta h} - U'\partial_x \bar{T} + \bar{W}\frac{T'_{\text{sub}}}{\Delta h} - V'\partial_y \bar{T} - W'\frac{\bar{T} - \bar{T}_{\text{sub}}}{\Delta h} \\ & -U'\partial_x T' - V'\partial_y T' - W'\frac{T' - T'_{\text{sub}}}{\Delta h} \\ & +k_l[\partial_{xx} T' + \partial_{yy} T'] + \partial_z \left[k_v(z) \frac{T' - T'_{\text{sub}}}{\Delta h} \right] + \frac{Q'_{\text{flux}}}{\rho_0 c_p h} + \frac{Q'_{\text{res}}}{\rho_0 c_p h} \end{aligned} \right] \quad (2)$$

The first three terms of the first line of equation (2) represent the dynamical damping from mean currents, the fourth term the zonal advective feedback, the fifth the thermocline feedback [Jin and An, 1999], and the two last terms the Ekman feedback [Jin and Neelin, 1993]. The terms on the second line represent the Nonlinear Dynamical Heating (NDH), i.e., (nonlinear) advection of temperature anomalies by anomalous currents [Jin et al., 2003], and the four terms of the last line represent respectively lateral mixing, vertical mixing, surface heat fluxes and a residual. Using a second-order Taylor expansion for the

heat fluxes $Q'_{\text{flux}}/(\rho c_p h) = \alpha T' + \beta T'^2$, multiplying each side of equation (2) by T' and taking a long-term average $\langle \cdot \rangle$, we obtain

$$0 = \left[\begin{aligned} & -\frac{1}{2} \bar{U} \partial_x \langle T'^2 \rangle - \frac{1}{2} \bar{V} \partial_y \langle T'^2 \rangle - \frac{\bar{W} \langle T'^2 \rangle}{\Delta h} - \langle T' U' \rangle \partial_x \bar{T} + \frac{\bar{W} \langle T' T'_{\text{sub}} \rangle}{\Delta h} \\ & - \langle T' V' \rangle \partial_y \bar{T} - \langle T' W' \rangle \frac{\bar{T} - \bar{T}_{\text{sub}}}{\Delta h} - \frac{1}{2} \partial_x \langle U' T'^2 \rangle - \frac{1}{2} \partial_y \langle V' T'^2 \rangle - \frac{\langle W' T'^2 \rangle - \langle W' T' T'_{\text{sub}} \rangle}{\Delta h} \\ & + \langle k_l T' [\partial_{xx} T + \partial_{yy} T'] \rangle + \left\langle T' \partial_z \left[k_v(z) \frac{T' - T'_{\text{sub}}}{\Delta h} \right] \right\rangle + \frac{\langle T' Q'_{\text{res}} \rangle}{\rho c_p h} + \alpha \langle T'^2 \rangle + \beta \langle T'^3 \rangle \end{aligned} \right] \quad (3)$$

Note that we have the alternative to either include the tendency term ($\langle \partial_t T'^2 \rangle$) in the residual or assume stationarity and simply disregard it. Over long timescales with multiple ENSO cycles, stationarity is a valid assumption, as long as all variables are linearly detrended. This is confirmed by a straightforward calculation of this term; $\langle \partial_t T'^2 \rangle$ eventually appears to be more than an order of magnitude smaller than the other feedbacks terms (supporting information Figure S4). The last terms $\langle T'^2 \rangle$ and $\langle T'^3 \rangle$ of equation (3) represent the variance σ^2 and the skewness of T' , respectively. The Ekman pumping term has been moved to the second line. Finally, we can express the variance of interannual ML temperature anomalies σ^2 , as the contribution of relevant ENSO feedbacks and its asymmetry:

$$\sigma^2 = -\frac{1}{\alpha} \left[\begin{aligned} & \text{Dynamical Damping} \quad \text{Zonal Advective feedback} \quad \text{Thermocline feedback} \\ & -\frac{1}{2} \bar{U} \partial_x \langle T'^2 \rangle - \frac{1}{2} \bar{V} \partial_y \langle T'^2 \rangle - \frac{\bar{W} \langle T'^2 \rangle}{\Delta h} - \langle T' U' \rangle \partial_x \bar{T} + \frac{\bar{W} \langle T' T'_{\text{sub}} \rangle}{\Delta h} \\ & \text{Ekman feedback} \quad \text{Nonlinear Dynamical Heating} \\ & - \langle T' V' \rangle \partial_y \bar{T} - \langle T' W' \rangle \frac{\bar{T} - \bar{T}_{\text{sub}}}{\Delta h} - \frac{1}{2} \partial_x \langle U' T'^2 \rangle - \frac{1}{2} \partial_y \langle V' T'^2 \rangle - \frac{\langle W' T'^2 \rangle - \langle W' T' T'_{\text{sub}} \rangle}{\Delta h} \\ & \text{Lateral Mixing} \quad \text{Vertical Mixing} \quad \text{Residual} \quad \text{Asymmetry} \\ & + \langle k_l T' [\partial_{xx} T + \partial_{yy} T'] \rangle + \left\langle T' \partial_z \left[k_v(z) \frac{T' - T'_{\text{sub}}}{\Delta h} \right] \right\rangle + \frac{\langle Q'_{\text{res}} T' \rangle}{\rho c_p h} + \beta \langle T'^3 \rangle \end{aligned} \right] \quad (4)$$

All terms in equation (4) are in the unit of $^\circ\text{C}^2$ due to the scaling of thermal damping coefficient α . Equation (4) is the basis of our diagnostic framework referred to as “Variance Heat Budget” (VHB). Unlike typical heat budget analysis, it allows determining the contribution of each term to the ML temperature variance (amplitude) over a long enough period of time and at any given location. All these contributions are relative to the second-order nonlinear damping rate between heat fluxes and local temperature anomalies. The higher-order couplings are absorbed into Q'_{res} . Note that our approach is different from the temperature variance budget of *Santoso et al.* [2010], in that we explicitly express the budget in terms of the actual variance while theirs expresses the variance tendency. Again, this is achieved by expanding $Q'_{\text{flux}}/(\rho c_p h)$ in terms of its first- and second-order coupling with near surface temperature, which allows a spatial evaluation of the budget without any more restrictive hypothesis.

2.2. Data

The VHB is then applied to the European Centre for Medium range Weather Forecasts (ECMWF) ocean analysis system (ORA-S3) over the period 1959–2009 [Balmaseda et al., 2008]. ORA-S3 is widely used within the climate community, in particular to study the tropical Pacific Ocean subsurface characteristics [e.g., Zhai and Hu, 2013; Jin et al., 2014]. As mentioned above, for the sake of simplicity, we assume a spatially and temporally constant mixed layer depth at 25 m (ORA-S3 third discretized vertical level) to average all heat budget terms. For our surface heat flux analysis, instead of using the original fluxes that were used to force ORA-S3, we choose the Objectively Analyzed air-sea Fluxes for the Global Oceans from the Woods Hole Oceanographic Institution (referred to as OA fluxes hereinafter) [Yu et al., 2008]. Indeed, the interpretation of ORA-S3 fluxes is not so trivial given the errors due to assimilation increments (i.e., the correction terms that take into account the misfits between model and observations).

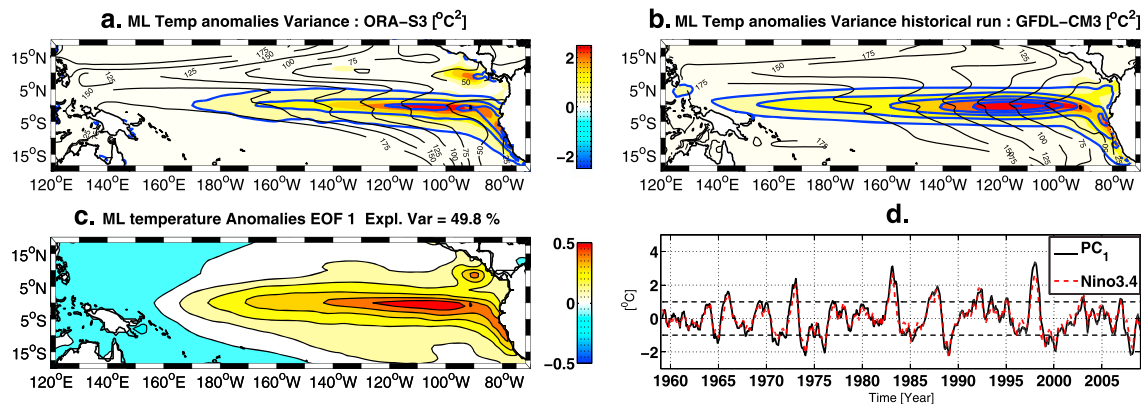


Figure 1. (a) Variance of interannual temperature anomalies averaged in a 25 m surface layer (shading) and at the surface (blue contours) for the period 1959–2009 from ORA-S3. Units are in $^{\circ}\text{C}^2$; dashed black lines represent the mean thermocline depth (depth of isotherms 20°C). (b) Same as Figure 1a but for the historical run of GFDL-CM3 (from CMIP5 database). The mixed layer is set constant at the discretized vertical level 25 m for ORA-S3 and GFDL-CM3. (c) First EOF mode of temperature anomalies averaged in the constant 25 m surface layer. (d) The associated time series (PC1), along with Niño3.4 time series (Surface temperature anomalies averaged in 160°E – 150°W , 5°S – 5°N).

These are partially due to errors in the forcing, but also errors in the model. In particular, the surface fluxes in ORA-S3 have been modified by the SST data through a strong nudging term. This term is largest in the upwelling areas, indicating that the heat flux correction is compensating for errors of dynamical origin. The non-negligible contribution of the assimilation heat fluxes is discussed in *Balmaseda et al.* [2013] (cf. Figure S5 in the supporting information). This is why we decide to employ an independent estimation of heat fluxes and use them for the analyses. To date, OA flux is one of the most reliable observationally based. To limit biases, the OA flux product combines flux variables from various reanalysis products, including ERA40, the atmospheric reanalysis from ECMWF that forces ORA-S3. The SST used in the OA fluxes bulk formula calculation is from the Advanced Very High Resolution Radiometer [Reynolds et al., 2007] and is coherent with ORA-S3 outputs (Root mean square errors of monthly SSTA are below 0.2°C all over the tropical Pacific except in the Peruvian upwelling region). Nonetheless, the key focus of our present study is essentially methodological. Sensitivity of the results to different reanalysis products should be explored in future studies. *Lübbecke and McPhaden* [2014] assess decadal changes in ENSO amplitude in a variety of ocean reanalysis products and even though they find a significant spread in terms of feedback strength, they found a robust behavior in terms of their relative contribution and decadal evolution.

Figure 1 compares the variance of SSTA (thick blue contours) and ML temperature anomalies (shading) from ORA-S3. They both exhibit a local maximum along the eastern equatorial Pacific associated with ENSO variability. However, in contrast to the SSTA variance, the ML temperature variance also increases in the northeastern tropical Pacific off the Costa Rican coast. This feature, which collocates with the mean thermocline depth (depth of isotherms 20°C , black contours), appears to be related to subsurface oceanic variability. The first EOF mode of ML temperature anomalies and its associated time series correlate significantly with Niño3.4 ($r=0.92$), revealing that temperature averaged over a constant shallow layer captures ENSO features well (Figures 1c and 1d), up to 50% of the amplitude of interannual anomalies is related to ENSO variability.

As a further motivation for our framework, we note that the pattern of the tropical Pacific temperature variance simulated by a typical state-of-the-art CGCM (GFDL-CM3) [Donner et al., 2011] is quite different from the ocean reanalysis product (Figure 1b). Apart from the westward bias in the pattern, which is common across global climate models [Li and Xie, 2014], the model also misses the northeastern tropical Pacific subsurface temperature variance maximum (Figure 1b shading; see also supporting information Figure S1). The latter may be related to the realism of the climatological thermocline depth that the CGCM also fails to realistically capture (Figure 1b, black contours). Understanding such model biases that are large-scale in pattern can be facilitated by analytical tools, such as the one developed here, which can quantify the effect of tropical climate feedbacks on interannual variability.

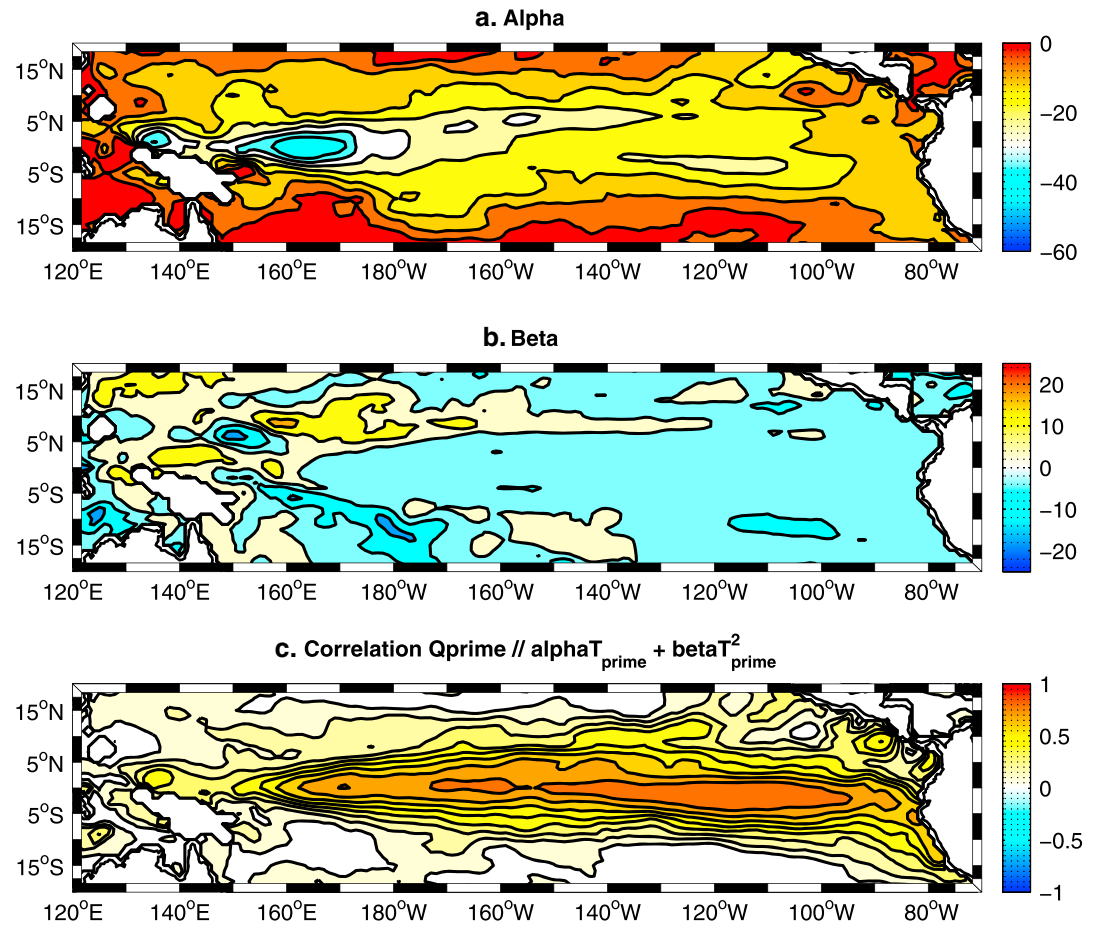


Figure 2. Nonlinear (second-order polynomial) regression of net heat flux onto surface layer temperature anomalies, i.e., $Q'_{\text{flux}} / (\rho c_p h) = \alpha T' + \beta T'^2$. Maps of (a) α (in s^{-1}), (b) β (in $\text{s}^{-1}\text{°C}^{-1}$), (c) regression skills, i.e., the correlation between Q'_{flux} and the regressed field $\alpha T' + \beta T'^2$.

3. Results

3.1. Mean VHB Over 1959–2009

Figure 2 shows the empirical coefficients α and β inferred from the second order polynomial regression of $Q'_{\text{flux}} / (\rho c_p h) = \alpha T' + \beta T'^2$, where $Q'_{\text{flux}} = Q'_{\text{short}} - Q'_{\text{long}} - Q'_{\text{sensible}} - Q'_{\text{latent}}$. The relative importance of these different heat fluxes on damping SST anomalies is discussed in the supporting information. Figure 2a shows that α is mostly negative over the tropical Pacific Ocean. The damping timescale $1/\alpha$ is similar to that used in conceptual studies [Jin *et al.*, 2006]. The coefficient β (Figure 2b) highlights areas of strong convection, mainly in the northwestern tropical Pacific and in the eastern part of the Pacific Warm Pool. The correlations in Figure 2c show a high fidelity of the quadratic fit between fluxes and ML temperature anomalies along the equator (correlations above 0.7 across the basin between 5°S and 5°N). Away from the equator, in region of strong convection, the score decreases substantially (correlations around 0.20). A similar quadratic regression has been performed using ORA-S3 original heat fluxes (supporting information Figure S5), which exhibits similar patterns but does not display such a good match across the equatorial basin, further justifying the use of the OA product. Note also that the strength of this damping relationship is particularly enhanced in the eastern Pacific (the key region for ENSO amplitude) when T' is integrated over a shallow layer (cf. supporting information Figure S3). Using this fit and the ORA-S3 data for T , U , V , W , h as well as the KPP parameterization for a horizontally homogenous $k_v(z)$, we can now calculate the individual terms of the VHB from equation (4).

The sum of all diagnosed terms (Figure 3i) reproduces the total surface layer temperature variance well which is largest in the main region of ENSO influence with errors representing less than 20% of the ML temperature

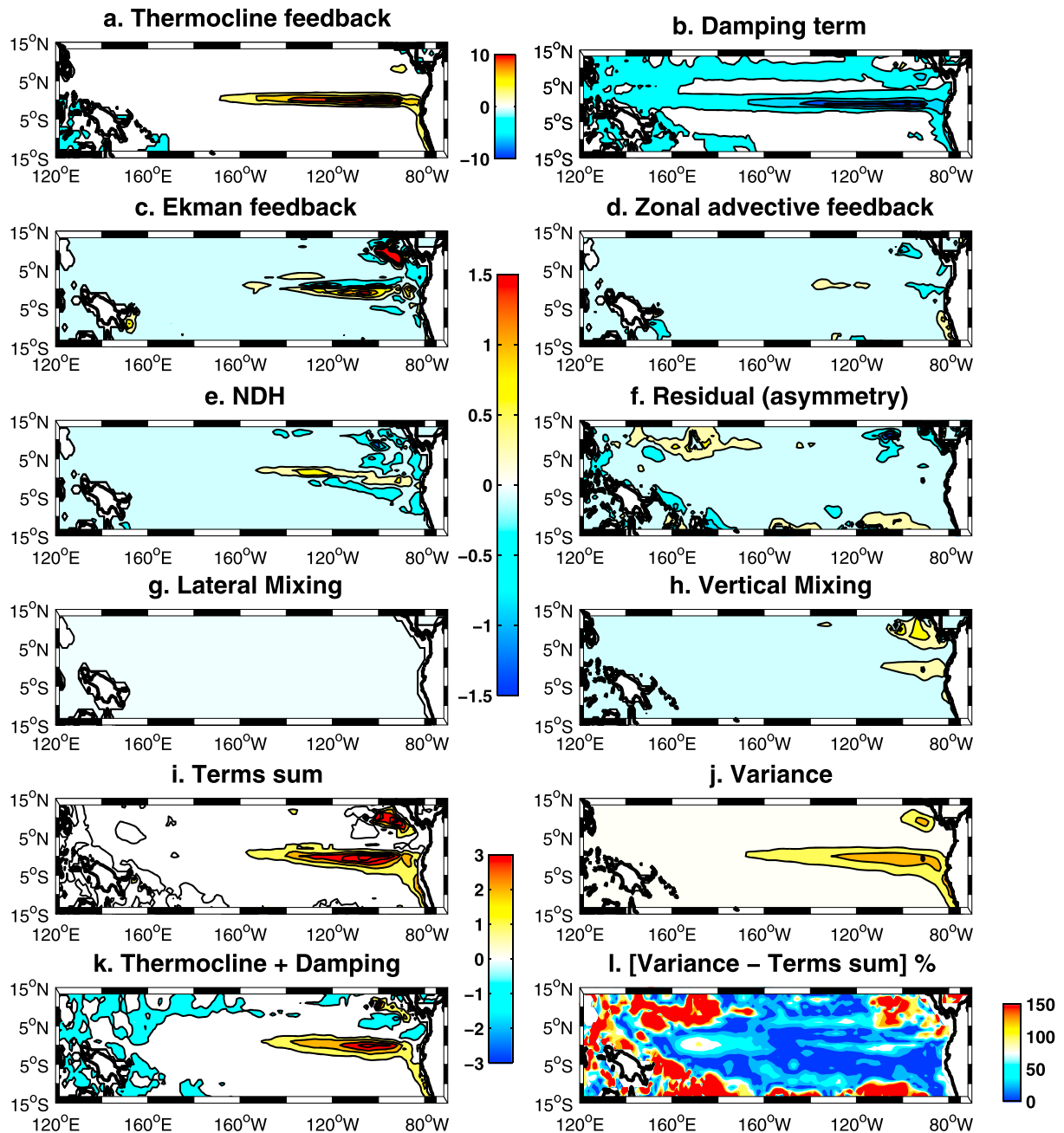


Figure 3. (a–h) Individual contributions of feedback terms to the mean surface layer temperature Variance Heat Budget (see equation (4)), (i) sum of terms (right-hand side of equation (4)), (j) variance of ML interannual anomalies (left-hand side of equation (4)), (k) the combination of the thermocline feedback and dynamical damping terms, and (l) percentage of errors between the variance and the sum of terms. All terms are in unit of $^{\circ}\text{C}^2$.

variance (Figure 3j). Studying the individual terms and their regional contributions, we find that the thermocline feedback is the dominant term for the ML temperature variance in the equatorial upwelling region (Figure 3a). The surface heat flux variance term (or dynamical damping, Figure 3b) weakens the effect of the thermocline feedback (Figure 3k). The zonal advection weakly contributes to ML temperature variance in the eastern tropical Pacific, in accordance with Jin *et al.* [2006], although the signal along the coast of Peru calls for further investigation of the upwelling dynamics on interannual timescales (Figure 3d). The Ekman feedback, associated with wind-stress curl anomalies, can generate local variance maxima off the equator and off the coast of Central America. In this region, the parameterized vertical mixing also significantly controls the variance (Figure 3h and supporting information Figure S2h). Other

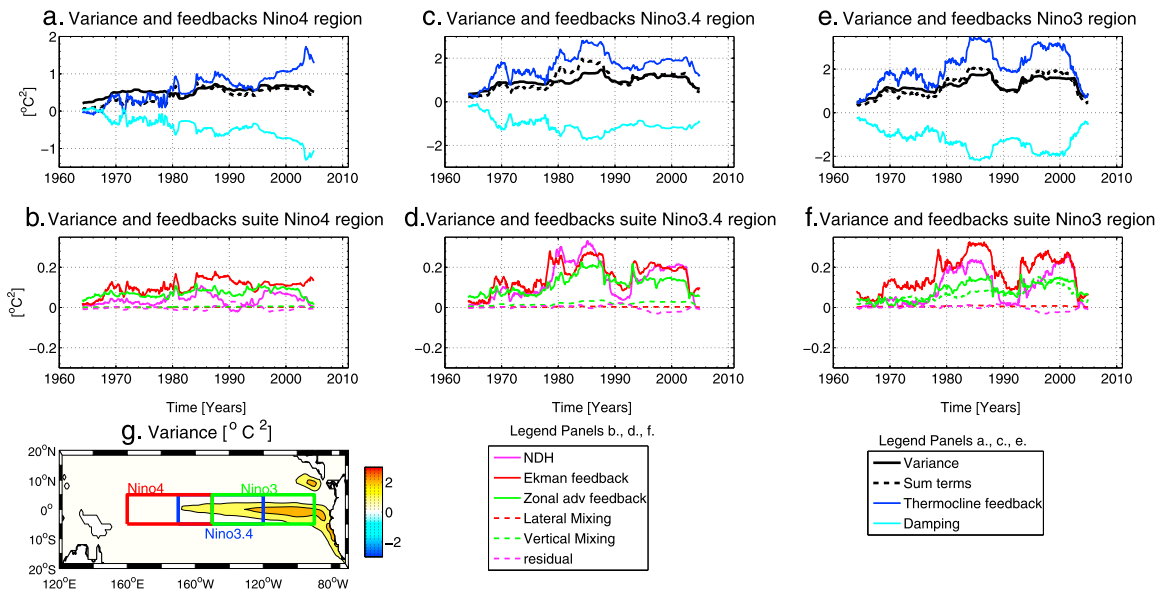


Figure 4. Individual spatially averaged contributions of feedback terms described in equation (4) to the 10 years running Variance Heat Budget ($^{\circ}\text{C}^2$) in (a and b) Niño4, (c and d) Niño3.4, and (e and f) Niño3. See text and (g) for definition of spatial averaging regions.

processes associated with lateral mixing and residual physics play only a secondary role for the observed ML temperature variance. NDH has been invoked to explain the positive skewness of ENSO [An and Jin, 2004; Jin et al., 2003] as well as the decadal bursting behavior of El Niño events [Timmermann and Jin, 2002; Timmermann et al., 2003]. The positive contribution of this term to ENSO variance is shown here to be restricted to a narrow equatorial region in the eastern Pacific.

In summary, this analysis shows that the VHB equation applied to the entire 1959–2009 period is a suitable tool for diagnosing the contribution of different dynamical processes in controlling local near surface temperature variability (Figure 3l). It should be noted that the VHB framework ignores several processes, such as time-varying mixed layer depth [Wang and McPhaden, 1999], higher frequency sub-monthly variability, and combination modes between annual cycle and ENSO's [Stuecker et al., 2013]. Whether these terms can explain the unresolved ML temperature north of the Galapagos Islands and along the eastern edges of the Warm Pool needs to be further resolved. Interestingly, these regions exhibit a small but non-vanishing tendency term (Supplementary Figure S4), which might reflect an effect of multidecadal signal on the stationarity hypothesis. In particular, in the central and western Pacific, this can be interpreted as the slow evolution of the Warm Pool mean characteristics, such as its deepening and eastward extension [Cravatte et al., 2009].

3.2. Low-Frequency Variability of ENSO Amplitude (Running VHB)

To determine why ENSO amplitude changes on decadal timescales, we apply the VHB method in a 10-year sliding window and subsequently average the different VHB terms over the Niño3 (150°W – 90°W ; 5°S – 5°N), Niño3.4 (120°W – 170°W ; 5°S – 5°N), and Niño4 (160°E – 150°W , 5°S – 5°N) regions. Since the OA fluxes used in the previous section only cover the period 1983–2009, we resort to the original ORA-S3 fluxes that span the total 1959–2009 period. Figure 4 shows the area-averaged contributions to the ML temperature variance. Similar to the long-term analysis, we find that even for the sliding windows, for which tendency terms can be slightly larger than those estimated for the entire period (see supporting information for results with a longer sliding window), the thermocline feedback and the dynamical damping explain most of the changes in temperature variance in the western (Figure 4a), central (Figure 4c), and eastern Pacific (Figure 4e). This is consistent with Borlace et al. [2013] who conclude that interdecadal modulation of ENSO variance is mostly controlled by the thermocline feedback strength in their 1000 years CGCM run. We also observe a contrasting behavior between the eastern and western equatorial Pacific that respectively displays a gradual decrease and intensification of the thermocline feedback and dynamical

damping over the last decade. Using the Bjerknes stability index [Jin *et al.*, 2006], Lübbecke and McPhaden [2014] also arrived at similar conclusions (supporting information Figure S10–S12). They link this robust weakening of the thermocline feedback in Niño3 region to a reduced thermocline slope associated with a fading wind stress response to eastern Pacific SST anomalies. The recent increase of the thermocline feedback in the central Pacific on the other hand can be attributed to an increase in equatorial vertical stratification that allows for a more effective influence of the thermocline depth fluctuations on the mixed-layer variability [Dewitte *et al.*, 2013]. The other main contributors to the variance modulation of ENSO across the equatorial Pacific are the zonal advective feedback, the NDH and the Ekman feedback (Figures 4b, 4d, and 4f). The Ekman feedback outweighs the contributions from the zonal advective feedback and the NDH, but not those of the thermocline feedback. Both the zonal advective feedback and NDH tend to be stronger in the Central and Eastern Pacific (Figures 4d and 4f) due to a stronger SST zonal gradient [Jin and An, 1999; Jin *et al.*, 2003]. Interestingly, the further east, the larger the contribution of the parameterized vertical mixing term. This is likely to be associated with a shallower mean thermocline and increased stratification. A more detailed analysis of the main drivers of the decadal modulation of ENSO variance in terms of background state changes or co-variance changes is beyond the scope of this brief letter.

4. Conclusions

The VHB diagnostic framework presented here helps to ascertain the contributions of climate feedbacks to local near surface temperature variance. Applied to the tropical Pacific and using ocean reanalysis data, we find that ENSO variance is largely controlled by the positive thermocline feedback and the negative dynamical damping feedback. Including a nonlinear feedback between temperature anomalies and heat flux changes allowed us to better capture the atmosphere/ocean heat fluxes in the convective warm pool regions. The sum of the diagnosed dynamical damping and thermocline feedback contributions to the variance accounts for a large fraction of the observed temperature variance in the eastern tropical Pacific. This suggests that irrespective of some simplifying assumptions (local relationship between temperature and heat flux, absence of high frequency, and combination tone contributions to the variance and a stationary ML depth), this method is successful in explaining local temperature variances.

Our method, which used monthly mean values of temperatures and ocean currents from ORA-S3, differs from the spatially averaged BJ index diagnostic developed by Jin *et al.* [2006] as it provides local information of dynamical feedbacks including tropical regions outside ENSO's main center of action. In particular, it allows highlighting unexpected dynamical characteristics such as the northeastern tropical Pacific and the Peruvian upwelling, where vertical mixing processes and the zonal advective feedback have respectively a strong contribution to ML variability (Figures 3d, 3h, and S2h).

The VHB method can be readily applied to diagnose variance changes in CGCM simulations, which will be helpful for diagnostic purposes and identification of model errors and ENSO sensitivities to external forcing. For future applications, we envision a more complete characterization of the ML temperature variance, by allowing for dynamic mixed layer changes to capture the entrainment processes. In addition, the role of higher-order processes or atmospheric and oceanic nonlinearities, for instance, can be studied further with respect to the main Bjerknes feedbacks. This can be done by moving collective variance terms $\langle T^2 \rangle$ and their gradients from the right-hand side to the left-hand side of equation (4).

References

- An, S.-I., and F.-F. Jin (2004), Nonlinearity and asymmetry of ENSO, *J. Clim.*, *17*, 2399–2412.
- An, S.-I., A. Timmermann, L. Bejarano, F.-F. Jin, F. Justino, Z. Liu, and A. W. Tudhope (2004), Modeling evidence for enhanced El Niño–Southern Oscillation amplitude during the Last Glacial Maximum, *Paleoceanography*, *19*, PA4009, doi:10.1029/2004PA001020.
- An, S.-I., Z.-Q. Ye, and W.-W. Hsieh (2006), Changes in the leading ENSO modes associated with the late 1970s climate shift: Role of surface zonal current, *Geophys. Res. Lett.*, *33*, L14609, doi:10.1029/2006GL026604.
- Ashok, K., S. K. Behera, S. A. Rao, H. Y. Weng, and T. Yamagata (2007), El Niño Modoki and its possible teleconnection, *J. Geophys. Res.*, *112*, C11007, doi:10.1029/2006JC003798.
- Balmaseda, M. A., A. Vidard, and D. L. T. Anderson (2008), The ECMWF Ocean Analysis System: ORA-S3, *Mon. Weather Rev.*, *136*, 3018–3034.
- Balmaseda, M. A., K. E. Trenberth, and E. Kallen (2013), Distinctive climate signals in reanalysis of global ocean heat content, *Geophys. Res. Lett.*, *40*, 1–6, doi:10.1002/grl.50382.
- Bellenger, H., E. Guilyardi, J. Leloup, M. Lengaigne, and J. Vialard (2013), ENSO representation in climate models: From CMIP3 to CMIP5, *Clim. Dyn.*, *42*, 1999–2018.

Acknowledgments

This project was supported by the Australian Research Council, US National Science Foundation grants ATM1034798, ATM1049219, and ATM1406601, US Department of Energy grant DESC005110, and US NOAA grant NA10OAR4310200. The Objectively Analyzed air-sea Fluxes for the Global Oceans from the Woods Hole Oceanographic Institution are available here: ftp://ftp.whoi.edu/pub/science/oaflux/data_v3/. Outputs from ORA-S3 reanalysis are available here: http://apdrc.soest.hawaii.edu:80/dods/public_data/Reanalysis_Data/ORA-S3/1x1_grid.

The Editor thanks two anonymous reviewers for assistance evaluating this manuscript.

- Borlace, S., W. Cai, and A. Santoso (2013), Multidecadal ENSO amplitude variability in a 1000-yr simulation of a coupled global climate model: Implications for observed ENSO variability, *J. Clim.*, **26**, 9399–9407.
- Boucharel, J., A. Timmermann, and F.-F. Jin (2013), Zonal phase propagation of ENSO sea surface temperature anomalies: Revisited, *Geophys. Res. Lett.*, **40**, 4048–4053, doi:10.1002/grl.50685.
- Cai, W., et al. (2015), Increased frequency of extreme La Nina events Under greenhouse warming, *Nat. Clim. Change*, **5**, 132–137, doi:10.1038/nclimate2492.
- Collins, M., et al. (2010), The impact of global warming on the tropical Pacific ocean and El Niño, *Nat. Geosci.*, **3**(6), 391–397.
- Cravatte, S., T. Delcroix, D. Zhang, M. McPhaden, and J. Leloup (2009), Observed freshening and warming of the western Pacific Warm Pool, *Clim. Dyn.*, **33**, 565–589.
- Dewitte, B., S.-W. Yeh, B.-K. Moon, C. Cibot, and L. Terray (2007), Rectification of the ENSO variability by interdecadal changes in the equatorial background mean state in a CGCM simulation, *J. Clim.*, **20**(10), 2002–2021.
- Dewitte, B., S.-W. Yeh, and S. Thual (2013), Reinterpreting the thermocline feedback in the western-central equatorial Pacific and its relationship with the ENSO modulation, *Clim. Dyn.*, **41**(3–4), 819–830.
- DiNezio, P. N., A. C. Clement, G. A. Vecchi, B. J. Soden, and B. P. Kirtman (2009), Climate response of the equatorial Pacific to global warming, *J. Clim.*, **22**(18), 4873–4892.
- DiNezio, P. N., B. P. Kirtman, A. C. Clement, S. K. Lee, G. A. Vecchi, and A. Wittenberg (2012), Mean climate controls on the simulated response of ENSO to increasing greenhouse gases, *J. Clim.*, **25**(21), 7399–7420.
- Donner, L. J., et al. (2011), The dynamical core, physical parameterizations, and basic simulation characteristics of the atmospheric component AM3 of the GFDL global coupled model CM3, *J. Clim.*, **24**(13), 3484–3519.
- Fedorov, A. V., and S. G. Philander (2000), Is El Niño changing?, *Science*, **288**, 1997–2002.
- Guilyardi, E., W. J. Cai, M. Collins, A. Fedorov, F.-F. Jin, A. Kumar, D.-Z. Sun, and A. Wittenberg (2012), New strategies for evaluating ENSO processes in climate models, *Bull. Am. Meteorol. Soc.*, **93**(2), 235–238.
- Jin, F.-F., and J. D. Neelin (1993), Modes of interannual tropical ocean–atmosphere interaction—A unified view. 1. Numerical results, *J. Atmos. Sci.*, **50**, 3477–3503.
- Jin, F.-F., and S.-I. An (1999), Thermocline and zonal advective feedbacks within the equatorial ocean recharge oscillator model for ENSO, *Geophys. Res. Lett.*, **26**, 2989–2992, doi:10.1029/1999GL002297.
- Jin, F.-F., S.-I. An, A. Timmermann, and J. Zhao (2003), Strong El Niño events and nonlinear dynamical heating, *Geophys. Res. Lett.*, **30**(3), 1120, doi:10.1029/2002GL016356.
- Jin, F.-F., S. T. Kim, and L. Bejarano (2006), A coupled-stability index of ENSO, *Geophys. Res. Lett.*, **33**, L23708, doi:10.1029/2006GL027221.
- Jin, F.-F., J. Boucharel, and I. I. Lin (2014), Eastern Pacific Tropical Cyclones intensified by El Niño delivery of subsurface ocean heat, *Nature*, **516**, 82–85.
- Kim, S. T., and F. F. Jin (2011), An ENSO stability analysis. Part II: Results from the twentieth and twenty-first century simulations of the CMIP3 models, *Clim. Dyn.*, **36**, 1609–1627.
- Li, G., and S.-P. Xie (2014), Tropical biases in CMIP5 multimodel ensemble: The excessive equatorial Pacific cold tongue and double ITCZ problems, *J. Clim.*, **27**, 1765–1780.
- Li, X., Y. Chao, J. C. McWilliams, and L.-L. Fu (2001), A comparison of two vertical-mixing schemes in a Pacific Ocean general circulation model, *J. Clim.*, **14**, 1377–1398.
- Lübbecke, J. F., and M. J. McPhaden (2014), Assessing the twenty-first-century shift in ENSO variability in terms of the Bjerknes Stability Index, *J. Clim.*, **27**(7), 2577–2587.
- McPhaden, M. J., et al. (1998), The Tropical Ocean-Global Atmosphere (TOGA) observing system: A decade of progress, *J. Geophys. Res.*, **103**(14), 169–240.
- Reynolds, R. W., T. M. Smith, C. Liu, D. B. Chelton, K. S. Casey, and M. G. Schlax (2007), Daily high-resolution-blended analyses for sea surface temperature, *J. Clim.*, **20**, 5473–5496.
- Santoso, A., A. S. Gupta, and M. H. England (2010), Genesis of Indian Ocean mixed layer temperature anomalies: A heat budget analysis, *J. Clim.*, **23**, 5375–5403.
- Santoso, A., S. McGregor, F.-F. Jin, W. Cai, M. H. England, S.-I. An, M. J. McPhaden, and E. Guilyardi (2013), Late 20th century emergence of El Niño propagation asymmetry and future projections, *Nature*, **504**, 126–130.
- Stuecker, M. F., A. Timmermann, F.-F. Jin, S. McGregor, and H.-L. Ren (2013), A combination mode of the annual cycle and the El Niño/Southern Oscillation, *Nat. Geosci.*, **6**(7), 540–544.
- Su, H., J. D. Neelin, and C. Chou (2001), Tropical teleconnection and local response to SST anomalies during the 1997–1998 El Niño, *J. Geophys. Res.*, **106**(D17), 20,025–20,043, doi:10.1029/2000JD000124.
- Timmermann, A. (2001), Changes of ENSO stability due to greenhouse warming, *Geophys. Res. Lett.*, **28**(10), 2061–2064, doi:10.1029/2001GL012879.
- Timmermann, A., and F.-F. Jin (2002), A nonlinear mechanism for decadal El Niño amplitude changes, *Geophys. Res. Lett.*, **29**(1), 1003, doi:10.1029/2001GL013369.
- Timmermann, A., F.-F. Jin, and J. Abshagen (2003), A nonlinear theory for El Niño bursting, *J. Atmos. Sci.*, **60**(1), 152–165.
- Vecchi, G. A., and B. J. Soden (2007), Global warming and the weakening of the tropical circulation, *J. Clim.*, **20**(17), 4316–4340.
- Wang, W., and M. J. McPhaden (1999), The surface-layer heat balance in the equatorial Pacific Ocean. Part I: Mean seasonal cycle, *J. Phys. Oceanogr.*, **29**, 1812–1831.
- Yeh, S.-W., J.-S. Kug, B. Dewitte, M.-H. Kwon, B. P. Kirtman, and F.-F. Jin (2009), El Niño in a changing climate, *Nature*, **461**, 511–514.
- Yu, L., X. Jin, and R. A. Weller (2008), Multidecade global flux datasets from the Objectively Analyzed Air-sea Fluxes (OAFlux) project: Latent and sensible heat fluxes, ocean evaporation, and related surface meteorological variables, *Woods Hole Oceanographic Institution, OAFlux Project Tech. Rep.*, OA-2008-01, 64 pp., Woods Hole, Mass.
- Zebiak, S. E., and M. A. Cane (1987), A model of El Niño–Southern Oscillation, *Mon. Weather Rev.*, **115**, 2262–2278.
- Zhai, F., and D. Hu (2013), Revisit the interannual variability of the North Equatorial Current transport with ECMWF ORA-S3, *J. Geophys. Res. Oceans*, **118**, 1349–1366, doi:10.1002/jgrc.20093.
- Zhang, W.-J., F.-F. Jin, H.-L. Ren, J.-P. Li, and J.-X. Zhao (2012), Differences in teleconnection over the North Pacific and rainfall shift over the USA Associated with two types of El Niño during boreal autumn, *J. Meteorol. Soc. Jpn.*, **90**(4), 535–552.